

Center vortices on $SU(2)$ lattices

A. Alexandru¹ and Richard W. Haymaker²

*Department of Physics and Astronomy, Louisiana State University,
Baton Rouge, Louisiana 70803-4001, U.S.A.*

e-mail addresses: ¹alexan@rouge.phys.lsu.edu, ²haymaker@rouge.phys.lsu.edu

Abstract

We show that gauge invariant definitions of thin, thick and hybrid center vortices, defined by Kovacs and Tomboulis on $SO(3) \times Z(2)$ configurations, can also be defined in $SU(2)$. We make this connection using the freedom of choosing a particular $SU(2)$ representative of $SO(3)$. We further show that in another representative the Tomboulis $\sigma - \eta$ thin vortices are P (projection) vortices. The projection approximation corresponds to dropping the perimeter factor of a Wilson loop after appropriate gauge fixing. We present results for static quark potentials based on these vortex counters and compare projection vortex counters with gauge invariant ones on the same configuration.

PACS indices:

11.15.Ha,

11.30.Ly.

1 Introduction

Given the possibility that $SU(N)$ center vortices occur abundantly in the vacuum of an $SU(N)$ lattice gauge theory then a simple mechanism emerges that may account for color confinement. A Wilson loop that links the core but lies in the asymptotic tail of the vortex would pick up a factor of $Z(N)$ compared to a configuration without this singular gauge transformation. If the cost of action of inserting this vortex is minimal then averages could be disordered by a mechanism that is proportional to the area of the loop. This has led to many recent efforts to understand vortices in the vacuum of QCD[1, 2, 3, 4].

Efforts to confirm this picture on the lattice remain problematic. Kovacs and Tomboulis[5] were able to confirm that a center vortex in $SU(2)$ could survive in the continuum limit at vanishing cost of action. In this example the center vortex is topologically trapped by twisted boundary conditions and there is no doubt about its presence. But it is not simple to establish the presence of a center vortex in an $SU(N)$ lattice configuration that is not trapped.

In addition to these structures, there are thin vortices associated with negative plaquettes costing action proportional to the area of the vortex sheet. Contrary to the above case these are suppressed in the continuum limit.

Some time ago, Tomboulis[6] developed a formalism that discriminates between these two structures. In this alternative partition function, the links, $U(b)$, are elements of $SU(2)$ but the action is invariant under sign flips of the links. Consequently, the two equivalent link values correspond to two equivalent *representatives* of $SO(3)$. The $Z(2)$ factor group is manifest on new independent variables $\sigma(p)$ living on plaquettes. The bookkeeping arising from the change in representatives is carried by $Z(2)$ valued dependent variables $\eta(p) = \text{sign tr}[U(\partial p)]$.

Recently we studied the configuration space of this formulation further in order to do simulations in these variables[7]. We found an ergodic algorithm for simulations on lattices with periodic and twisted boundary conditions. In Section 2 of this paper we find a mapping between these variables and the usual $SU(2)$ link variables, $U(b)$. The key is to identify a specific representative which gives a correspondence between the two configurations. As a consequence, the operators specific to the Tomboulis configurations can be measured on

$SU(2)$ configurations as we show in Section 3.

In the Tomboulis formulation, negative values of $\eta(p)\sigma(p)$ are constrained to form closed vortex sheets that we denote as $\sigma - \eta$ vortices. In general, the two species form patches denoted by σ and η . Although pure σ vortices are ruled out as contributors to the continuum string tension, the disordering signal from the σ patches alone give a string tension that *increases* in approach to the continuum limit[7, 8]. In Section 4 we give numerical confirmation of this and resolve the connection between this result and known scaling results.

These results allow for a direct comparison of these gauge invariant vortex counters with those defined by the projection vortex algorithm[1]. It is also interesting to note that in a particular representative the projection vortices themselves are present in the Tomboulis formulation. We describe this in Section 5. In Section 6 we look for coincidences between these two types of vortices.

2 $SU(2)$ configurations in $SO(3) \times Z(2)$ variables

In ref[7] we rederived the Tomboulis $SO(3) \times Z(2)$ form[2] for the $SU(2)$ partition function. Let us consider only periodic boundary conditions, eliminating complications due to a twist.

$$Z = \sum_{\sigma(p)} \int [dU(b)] \prod_c \delta(\sigma(\partial c)\eta(\partial c)) \exp\left(\beta \sum_p \frac{1}{2} |\text{tr}[U(\partial p)]| \sigma(p)\right), \quad (1)$$

where

$$\text{tr}[U(\partial p)] = \eta(p) |\text{tr}[U(\partial p)]|. \quad (2)$$

The $\sigma(p)$ are a new set of independent variables living on plaquettes. The $m \times n$ Wilson loop in these variables includes tiling factors $\sigma(p)$ and $\eta(p)$,

$$W_{m \times n} = \text{tr}[U(C)] \eta(S) \sigma(S) |_{C=\partial S}, \quad (3)$$

$$P = W_{1 \times 1} = \text{tr}[U(\partial p)] \eta(p) \sigma(p) = |\text{tr}[U(\partial p)]| \sigma(p), \quad (4)$$

where S is any surface that spans C . Note that $\sigma(p)$ gives the sign of the plaquette. The delta function constraint enforces an even number of negative $\sigma(p)$ or $\eta(p)$ faces on all

cubes. As a consequence, the elementary excitations of these $Z(2)$ valued variables taken together from co-closed vortex sheets. We denote these in general as $\sigma - \eta$ vortices which in the degenerate cases are pure σ or pure η vortices. The partition function, Eqn.(1), is invariant under sign flips of the links. On a lattice with n links there are 2^n *representatives* of the $SO(3)$ symmetry obtained by flipping the signs of the links. Such a transformation flips the sign of the 6 $\eta(p)$'s forming the co-boundary of a link. This in turn will result in 0 or 2 sign flips for all cubes, leaving the constraint satisfied. This process will either create an elementary vortex of negative $\eta(p)$'s or deform an existing vortex. The plaquette and all Wilson loops are invariant under this operation.

One can reach all configurations through local updates of the independent variables $U(b)$ and $\sigma(p)$ while maintaining the cube constraint[7]. Starting from a configuration in which the cube constraint is satisfied, e.g. a cold configuration, (i) one first updates the links $U(b)$. If the sign of $\text{tr}[U(\partial p)]$ in the co-boundary of the link flips then $\eta(p)$ also flips. The cube constraint will be maintained if one also flips the sign of the corresponding $\sigma(p)$. Second, (ii), flip the sign of all six $\sigma(p)$'s forming the co-boundary of each link. This will also maintain the constraint.

We now want to relate these configurations to $SU(2)$. Using the freedom of choosing a representative we can modify the algorithm. Note that in step (i) a negative $\eta(p)$ is always accompanied by a corresponding negative $\sigma(p)$. We can modify step (ii) so that this property holds there too. This is achieved by flipping the sign of the link $U(b)$ that defines the six co-boundary plaquettes. This would flip the signs of the corresponding six $\eta(p)$'s.

This particular choice of representative maps the $SO(3) \times Z(2)$ configurations to $SU(2)$. Note that in this representative, denoted $\tilde{U}(b)$, $\eta(p)\sigma(p) = 1$, and the cube constraint, Eqn.(1), is automatically satisfied. Hence Z simplifies to

$$\tilde{Z} = \int [d\tilde{U}(b)] \exp \left(\beta \sum_p \frac{1}{2} \text{tr}[\tilde{U}(\partial p)] \right), \quad (5)$$

The Wilson loops also simplify

$$W_{m \times n} = \text{tr}[\tilde{U}(C)].$$

Further, this particular representative is characterized by the fact that there are no $\sigma - \eta$

vortices since negative σ 's are paired with negative η 's.

$$\tilde{U}(b) \iff U^{SU(2)}(b) \iff (\sigma - \eta) \text{ vortices absent} \quad (6)$$

The $SU(2)$ and $SO(3) \times Z(2)$ local update algorithms are known independently to be ergodic, and since there is a correspondence between the two in a particular representative, then the difference between the two link configurations, simply reflects the difference in representatives.

From a practical point of view this means that we can use the less cumbersome $SU(2)$ updates to produce configurations and then use the $SO(3) \times Z(2)$ formalism to explore representatives and the corresponding vortex structure.

3 Kovacs-Tomboulis vortex counters in $SU(2)$

We have seen in the previous section how to generate the $SO(3) \times Z(2)$ configurations using the regular $SU(2)$ algorithm. We show here how to measure the operators defined by Kovacs and Tomboulis[2] on the equivalent $SU(2)$ configurations.

First, let us review these definitions. The sign of the Wilson loop is given by three components: a σ tiling, an η tiling and the sign of the contour. They defined three vortex counters describing the number of vortices $mod(2)$ linking a particular Wilson loop

$$\begin{aligned} N_{thin}(S) &= \sigma(S), & \sigma(S) &= \prod_{p \in S} \sigma(p), \\ N_{thick}(S) &= \text{sign tr}[U(C)] \eta(S), & \eta(S) &= \prod_{p \in S} \eta(p), \\ N_{hybrid} &= N_{thin}(S) \times N_{thick}(S) = \text{sign } W_{m \times n}. \end{aligned}$$

The first two counters depend on the surface chosen to tile the Wilson loop. The hybrid counter is just the product of the first two counters and it is independent of the surface S . Thus N_{thin} and N_{thick} change sign simultaneously as we change the surface S . If N_{thin} or $N_{thick} = -1$ for all surfaces tiling the Wilson loop then we have a pure *thin* or *thick* vortex linking with the Wilson loop (or an odd number of them). If they change value as we change S but $N_{hybrid} = -1$ then we have a *hybrid* vortex (or an odd number of them) linking the Wilson loop.

This set of operators can be defined on $SU(2)$ configurations. Following the same argument as above we take a $SO(3) \times Z(2)$ configuration in the particular representative that has no σ - η vortices, denoted $\tilde{U}(b)$ in Eqn(6). Since for every plaquette with $\sigma(p) = -1$ we also have $\eta(p) = \text{tr}[\partial\tilde{U}(p)] = -1$, the $SU(2)$ operator for σ is

$$\sigma^{SU(2)}(p) = \text{sign tr}[\partial\tilde{U}(p)].$$

Using this we can define the thin vortex counter on $SU(2)$ configurations to be

$$N_{thin}^{SU(2)}(S) = \prod_{p \in S} \text{sign tr}[\partial\tilde{U}(p)].$$

We have already noted that the hybrid counter is the sign of the Wilson loop and thus we have

$$N_{hybrid}^{SU(2)} = \text{sign tr}[\tilde{U}(C)].$$

To define the thick counter we use the fact that $N_{thick}(S) = N_{thin}(S) \times N_{hybrid}$,

$$N_{thick}^{SU(2)}(S) = \prod_{p \in S} \text{sign tr}[\partial U(p)] \times \text{sign tr}[U(C)].$$

Although the presentation here was more intuitive than rigorous it is easy to show that these operators are indeed equivalent in the sense that they have the same average on $SU(2)$ configurations as the original vortex counters on $SO(3) \times Z(2)$ configurations and similarly for polynomial functions.

We can measure these operators using standard $SU(2)$ simulations. In the next section we investigate the interquark potential based on these counters. Furthermore, we can now compare these vortices with P vortices on the same configuration which we do in the last two sections.

4 Vortex Potentials

Although it is straightforward to measure N_{thin} , N_{thick} and N_{hybrid} , it is highly problematic to correlate these measurements with linkings of the corresponding species of vortex. This is because of the proviso that the value be independent of surface. It is very time consuming to generate all possible surfaces that tile a particular Wilson loop. Moreover, in a configuration

that has *monopoles* (cubes where the product of σ on all six face is negative) these pure vortex counters are difficult to define. According to the above definition all vortices are hybrid. Due to these problems we restrict our attention to only the minimal surface to define the vortex counters with the understanding that it is ambiguous. If, for example, the *thin* vortex counter = -1 for the minimal surface then we detect either a trapped *thin* or *hybrid* vortex. We expect that averages of these operators are independent of surface.

To extract the vortex potentials we measured the Wilson loops and vortex counters at $\beta = 2.3, 2.4$ and 2.5 on a 22×14^3 lattice, using 3000, 1000 and 1228 configurations respectively. We thermalized using 1000 updates and the measurements were separated by 40 updates. The acceptance was calibrated to be approximately 50%.

The contribution to the potential from the three types of vortex counters is

$$V_{counter}(R) = - \lim_{T \rightarrow \infty} \frac{1}{T} \ln \langle N_{counter}(W(R, T)) \rangle,$$

where $N_{counter}(W(R, T))$ is the counter signal for that particular Wilson loop (taking values ± 1). To determine the potential for a particular R we use Wilson loops $W(R, T)$ and an array of T 's that are large enough for the exponential behavior to set in and do a fit with an exponential in T .

We extracted the string tension, σ , and checked scaling by fitting these data with the function

$$V(r) = \sigma r - \frac{e}{r} + V_0,$$

where e/r represents the Coulomb part of the potential at short distances and V_0 is a self-energy. The parameters σ and e are expected to scale whereas V_0 which depends strongly on the cut-off is not expected to scale. Using the physical value of the string tension $\sigma = (440 MeV)^2$ we determine the lattice spacing. The results are in the Table 1.

In Fig. 1 we present the scaling graphs for the potentials extracted using the vortex counters. We see that the hybrid potential scales since it follows exactly the full potential. This was first noticed by Kovacs and Tomboulis [2].

We also see that the potential generated by the thick counter differs substantially from the full potential. This is contrary to our expectations since we expected that the thick counter would show a behavior very much like the hybrid counter. We show below that this is a consequence of the existence of thin patches in the hybrid vortices.

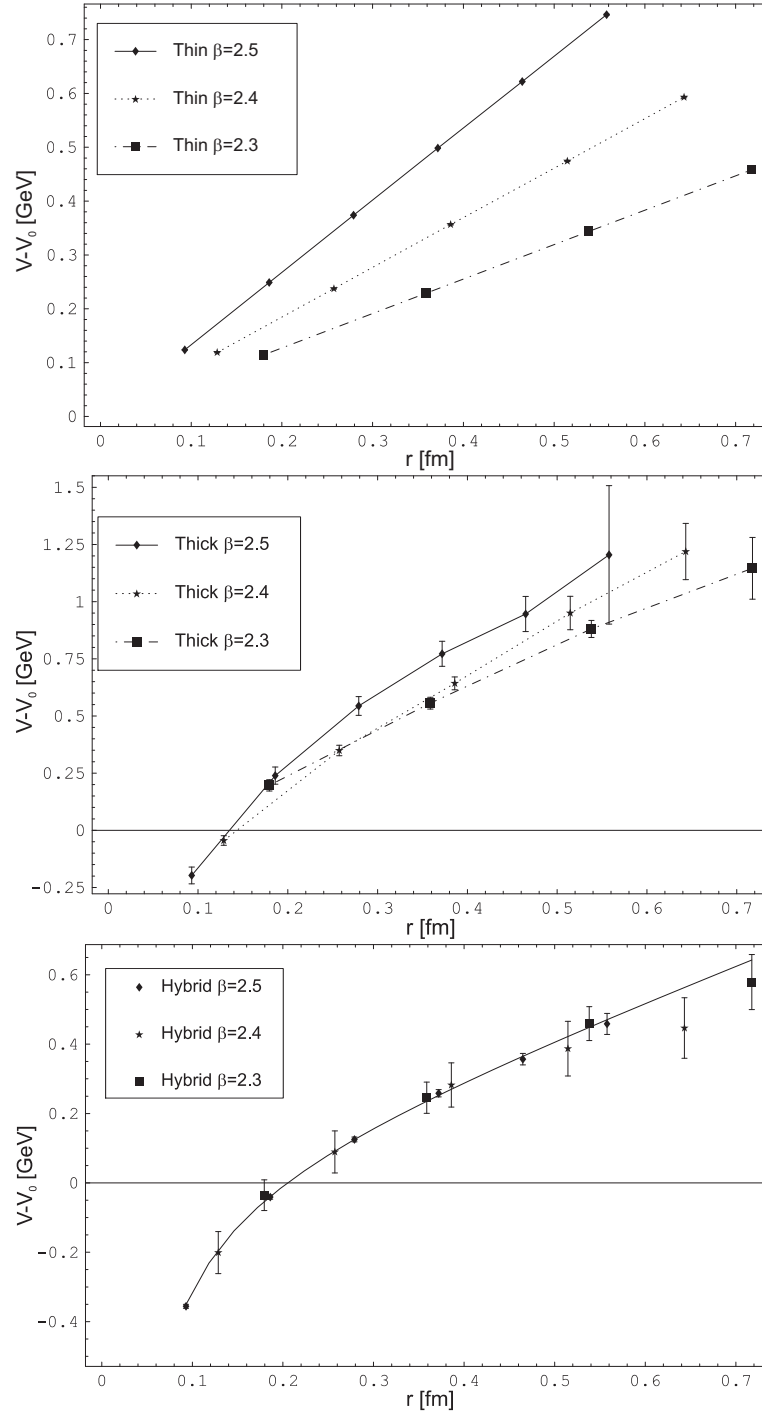


Figure 1: Vortex potentials in physical units: thin (top), thick (middle), hybrid (bottom). The line in the hybrid plot represents a fit.

Table 1: String tension and lattice spacing.

β	σ [lattice units]	lattice spacing [fm]	e [natural units]	V_0 [GeV]
2.3	0.157(14)	0.177(8)	0.193(25)	0.51(11)
2.4	0.083(10)	0.129(8)	0.217(24)	0.78(20)
2.5	0.043(1)	0.093(2)	0.211(3)	1.07(6)

The thin counter produces a very clear string tension. This agrees with our observation [7, 8] of the string tension in the Wilson loop tagged by thick vortices (the string tension there was roughly 1.1 where the string tension at $\beta = 2.3$ extracted from thin potential is 1.043(1)).

However note that the thin and thick potentials do not scale. Moreover, we see from these plots very clearly that the thin potential string tension increases in physical units rather than vanishing[7, 8]. Thus the potential produced by thin patches, although not relevant for confinement, cannot be disregarded. The fact that the string tension due to the thin patches does not vanish as we approach the continuum limit is also producing a non-scaling behavior for the thick potential. To see this we write down the hybrid counter:

$$N_{hybrid} = N_{thin} \times N_{thick}$$

If the thin and thick counters were completely uncorrelated then we would expect that:

$$\langle N_{hybrid} \rangle = \langle N_{thin} \rangle \times \langle N_{thick} \rangle$$

Since we know now that $\langle N_{thin} \rangle \sim e^{-\sigma A}$, with increasing σ (in physical units) as we approach the continuum limit, the hybrid counter would also have a non-physical string tension. However, we know that the hybrid potential scales properly (since it behaves exactly like the full potential) and thus the thin and thick counters cannot be uncorrelated[8].

The correlation comes from the hybrid vortices since our counters measure the signal only on a single surface. A hybrid vortex produces a thin or thick signal depending on how it pierces the minimal surface. Thus both the thin and thick counters includes extraneous signals due to hybrid vortices. Since we believe that the pure thin vortices cannot produce any string tension as we approach the continuum limit we assume that the string tension

that we see in the thin counters is due to these hybrid vortices (more precisely the thin patches in the hybrid vortices).

In order to see the properties of the pure thick vortices we need to remove the contribution due to the thin patches of hybrid vortices. One way to do it, if the above reasoning is true, is by subtracting the thin potential from the thick potential. In Fig. 2 we plot this difference. We see that apart from a constant the full potential and difference of the thick and thin potentials are the same. The string tension recovered from the scaling graph is the same within the error bars with the full string tension.

5 Projection Vortices

To define projection vortices, (P vortices) [1], one fixes to a standard gauge, e.g. the maximal center gauge. Let us set aside the specifics of gauge fixing.

There are two distinct ways to identify P vortices in $SO(3) \times Z(2)$ configurations giving the same result.

(i) After gauge fixing, one projects the full links $U(b)$ onto $Z(2)$ link variables $u(b)$, taking the values

$$\text{sign } \text{tr}[U(b)] \rightarrow u(b).$$

The negative plaquettes in this $Z(2)$ theory form co-closed surfaces, i.e. giving thin vortices. These would be the P vortices in an $SU(2)$ configuration. But that is not the case here.

The problem with this procedure is apparent in noting that changing representatives changes the locations of these vortices. The action is invariant under these transformations and hence the locations of these thin vortices are not uniquely defined.

In order to get P vortices we need to include $\eta(p)$ and $\sigma(p)$ tiling factors just as in the case of full Wilson loops, Eqn.(3). Therefore the P vortices are given by the occurrence of negative values of $u(p)$ where

$$u(p) = u(\partial p)\eta(p)\sigma(p) \tag{7}$$

where $\eta(p)$ and $\sigma(p)$ are defined in the unprojected full theory. This definition is representative independent in the same sense that the Wilson loop is in the full theory.

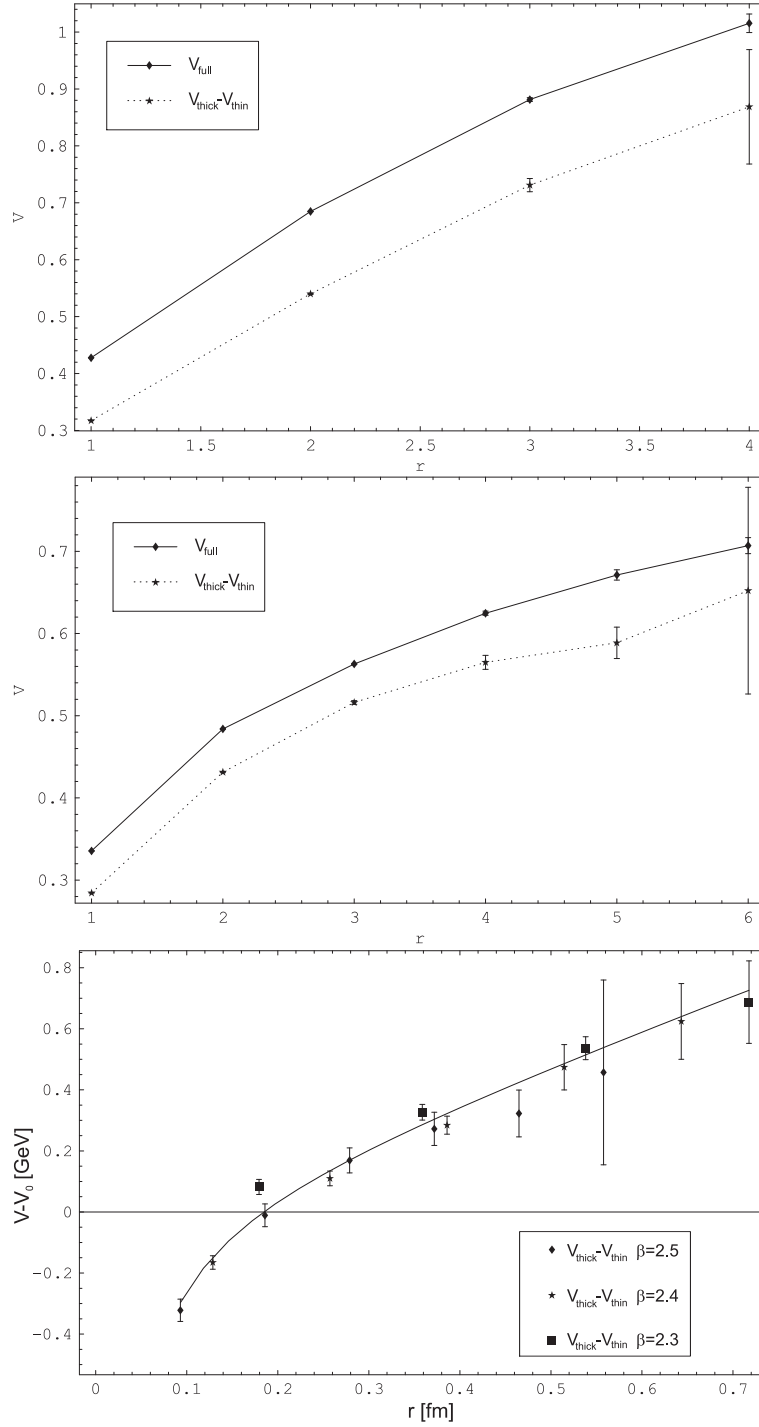


Figure 2: The difference between the thick and the thin potential plotted along with the full potential. The graphs at the top and middle are for $\beta = 2.3$ and $\beta = 2.5$ respectively. The bottom is both data sets on a scaling graph.

(ii) There is a simpler identification of P vortices that makes use of the freedom to choose a particular representative which we denote by $\widehat{U}(b)$. Starting with a given $SO(3) \times Z(2)$ configuration let us make a single sweep flipping the signs so that for all links

$$\text{tr}[\widehat{U}(b)] \geq 0.$$

In this representative the projected links, $u(b)$, are all positive and there are no negative values of $u(\partial p)$ and no vortices due to the $u(b)$ variables. But that means that the tiling factors themselves give the P vortices. The $\sigma - \eta$ vortices are already the P vortices themselves in this particular representative.

$$\widehat{U}(b) \iff (\sigma - \eta) \text{ vortices are the same as P vortices}$$

Although this gives the P vortices, there is as yet no approximation. One has transferred the sign from one factor to another making up the Wilson loop, Eqn.(3).

The approximation comes when one replaces

$$\text{tr}[\widehat{U}(C)] \rightarrow +1. \tag{8}$$

The success of this approximation is dependent on the success of the gauge fixing algorithm in transferring the confinement physics from the contour to the tiling factors.

6 Vortex Comparison

The K-T definition for vortices[2] is appealing since it is gauge invariant but they are hard to localize on a lattice. P vortices [1], on the other hand, are easy to localize but are not gauge invariant. It is interesting to see if these two definitions agree. We now have the tools to compare these definitions of vortex counters on the same configurations.

Our first test was to take a thermalized $SU(2)$ gauge configuration and project it. We fixed to the direct center gauge[1] without preconditioning[9] or simulated annealing[10] where the evidence for P vortex dominance is strongest. We measured the K-T counters on the original gauge configuration and the P vortex counter on the projected configuration. We counted only the fraction of loops of a certain size that produces a negative signal,

$$f_{counter} = \langle \frac{1}{2}(1 - N_{counter}) \rangle,$$

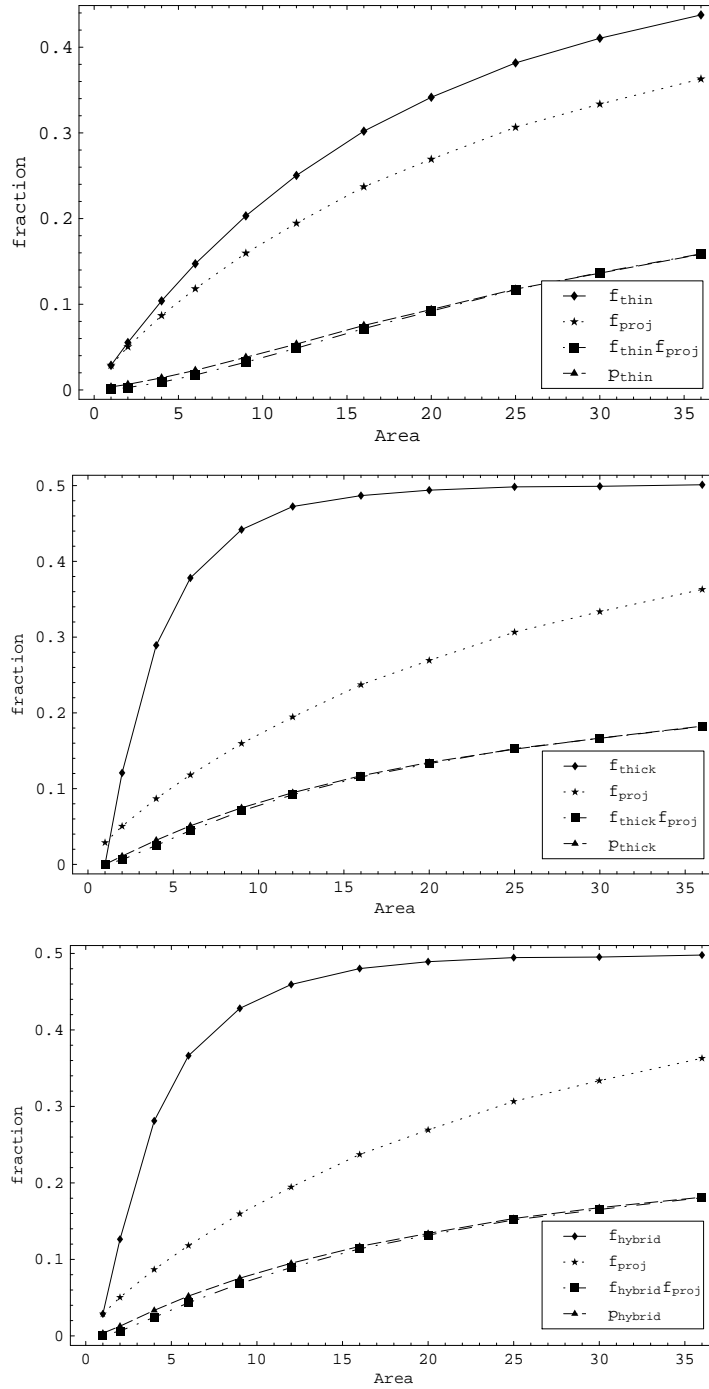


Figure 3: K-T counters and their coincidence with the P vortices. The p_{counter} is very close to the lower bound $f_{\text{proj}} \times f_{\text{counter}}$ which indicates no correlation.

where the counter can be thin, thick, hybrid or projection. We then measured the coincidence between the P vortex counter and one of the K-T counters. This measures the fraction of Wilson loops of a certain size that has both the P vortex counter and that particular K-T counter negative,

$$p_{counter} = \langle \frac{1}{2}(1 - N_{projection}) \times \frac{1}{2}(1 - N_{counter}) \rangle.$$

where the counter can be thin, thick or hybrid. If the vortices are completely uncorrelated then,

$$p_{counter} = \langle \frac{1}{2}(1 - N_{projection}) \rangle \times \langle \frac{1}{2}(1 - N_{counter}) \rangle = f_{projection} \times f_{counter}.$$

If they are completely correlated then,

$$p_{counter} = \min\{f_{projection}, f_{counter}\}.$$

These are the bounds on the coincidence counter. If the $p_{counter}$ approaches the lower bound $f_{proj} \times f_{counter}$ then the vortex counters are uncorrelated and we conclude that the physics that generates the counters is different. If the coincidence counter is closer to the upper bound then we conclude that the counters detect the same structures.

The results are presented in Fig. 3. We see that the counters show no correlation. This indicates that P vortices and K-T vortices are different objects.

However, there is another possibility which leads to our second test. The projection procedure can produce different results for gauge equivalent configurations. The argument is that when we have a thick center vortex the projection produces a P vortex somewhere inside the core. However, this P vortex can be anywhere inside the thick core depending on the gauge copy used. Thus the correlation signal might be lost due to P vortices fluctuating in and out of the perimeter.

To determine whether the perimeter produces the decorrelation we employed a method used to determine the self-correlation of P vortices [11]. We looked at products of the P vortex and K-T vortex counters,

$$\langle N_{counter}(W_{m \times n}) N_{projection}(W_{m \times n}) \rangle.$$

Each of the counters produces a string tension. If they are uncorrelated their product will exhibit a string tension equal to the sum of their string tensions. On the other hand, if they

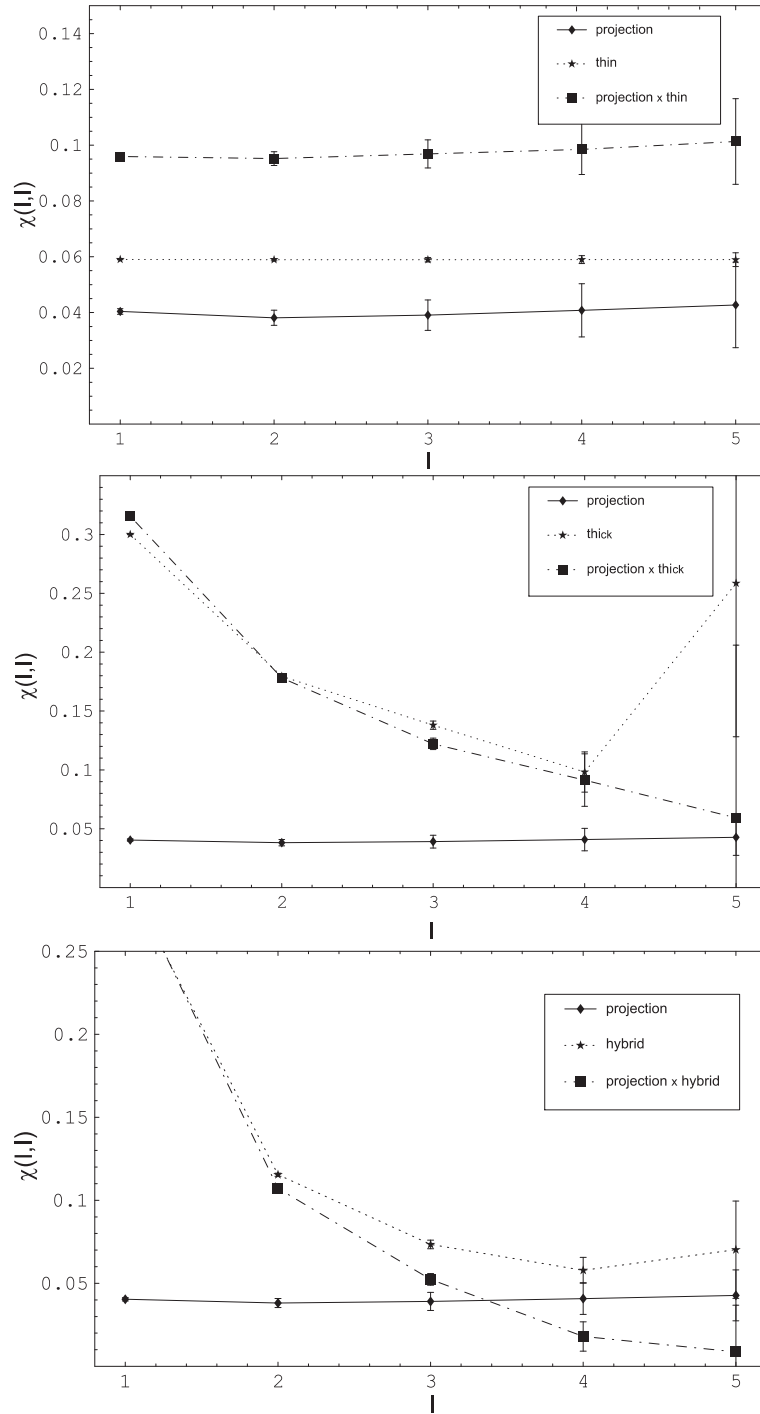


Figure 4: Creutz ratios for the products between the P vortex counter and K-T counters.

are correlated and identify the same vortices, and if the vortices they identify are indeed responsible for confinement then the product may have a perimeter behavior but will have no string tension.

In Fig. 4 we present the Creutz ratio for the products between the P vortices and Tomboulis vortices together with the Creutz ratios for each counter alone. Our simulation was run on a 16^4 lattice at $\beta = 2.5$. We used 1000 sweeps to thermalize the lattice and we made 1000 measurements separated by 40 updates.

We see from these graphs that the thin vortex counter shows no correlation with the P vortex counter. However, both thick and hybrid counters are showing a strong correlation with the P vortex counter.

In the case of the hybrid vortex counter we expected the correlation since we know that by eliminating P vortices the full Wilson loop loses the string tension [1, 11] and that the hybrid counter produces the same potential as the full Wilson loop [2]. The thick vortex correlation with the P vortex is due to the pure thick part of the counter. We know that the thick counter also includes a part due to thin patches and thus we don't expect the product of P vortex counter and thick counter to lose the string tension since we know that the thin vortex counter is uncorrelated with the P vortices. Our expectation is that this product will exhibit a string tension that is equal with the one generated by the product of thin vortex counter with the P vortex counter. Unfortunately, the precision of our data doesn't allow us to check if this is indeed true.

7 Summary and Conclusions

We have used the freedom of picking a representative to uncover some kinematical relationships. On the one hand we chose a representative, denoted $\tilde{U}(b)$ which eliminated $\sigma - \eta$ vortices allowing the mapping of the $SO(3) \times Z(2)$ configuration space onto $SU(2)$. And second by choosing another representative in which $\text{tr}[\hat{U}(b)] \geq 0$ for all links we found the $\sigma - \eta$ vortices to be identical to P vortices. The *projection approximation* has the added steps of gauge fixing and, after picking the representative, setting the contour integral $\text{tr}[\hat{U}(C)] = 1$.

It is interesting to note that it is not necessary to define an underlying $Z(2)$ gauge theory to identify P vortices. These structures are already present in the full $SO(3) \times Z(2)$ version of the theory.

We find it surprising that the string tension in the “thin potential” doesn’t vanish in the continuum limit. On the contrary it becomes larger. We argued that this must be due to thin patches of hybrid vortices. The counters measured on a single surfaces can not distinguish between the two.

We further see that there is a strong correlation between the thick and thin counters. The thick counter on a single surface can not distinguish thick vortices from thick patches of hybrid vortices. Hence as a corollary, we expect this anomalous string tension in the “thick potential” which we also see. This is further support that hybrid vortices are responsible.

By subtracting the “thin potential” from the “thick potential” we conjecture that we see the potential due to thick vortices alone. To see that this is indeed the potential due to pure thick vortices a more careful analysis is required. We need to first find a definition for pure thick vortices that works in a general configuration including those that have monopoles.

An alternative is to use the definition that we have now but generate configurations that have no monopoles. In such configurations we have only pure thin and thick vortices. It is very likely that in such an approach that the thick potential will be identical with the full potential (at least at large distances) since we expect that the pure thin vortices produce at best a perimeter law. The problem with this approach is that we are changing the dynamics of the system by forbidding the monopoles.

8 Acknowledgments

We are pleased to thank E. T. Tomboulis, S. Olejnik and S. Chelubaraja for helpful discussions. This work was supported in part by United States Department of Energy grant DE-FG05-91 ER 40617.

References

- [1] L. Del Debbio, M. Faber, J Greensite and S. Olejnik, Phys. Rev. **D** 55, 2298 (1997).
- [2] T. G. Kovacs and E. T. Tomboulis, Phys. Rev. **D** 57, 4054 (1998).
- [3] M. Engelhardt, K. Langfeld, H. Reinhardt, O. Tennert, Phys. Rev. **D** 61, 054504 (2000).
- [4] P. de Forcrand and M. Pepe, Nucl. Phys. **B** 598, 557 (2001)
- [5] T.G. Kovacs, E. T. Tomboulis, Phys. Rev. Lett. **85**, 704 (2000).
- [6] E.T. Tomboulis, Phys. Rev. **D23**, 2371 (1980).
- [7] A. Alexandru, R.W. Haymaker, Phys. Rev. **D62**, 074509 (2000).
- [8] A. Alexandru, R.W. Haymaker, Nucl. Phys. (Proc. Suppl.) **94** 543 (2001).
- [9] T. G. Kovacs and E. T. Tomboulis, Phys. Lett. **B** 463, 104 (1999).
- [10] V. Bornyakov, D. Komarov, M. Polykarpov, Phys. Lett. **B497**, 151 (2001).
- [11] L. Del Debbio, M. Faber, J. Giedt, J. Greensite, S. Olejnik, phys. Rev. **D** 58 094501 (1998).